Bulletin of the Seismological Society of America, 91, 3, pp. 561–571, June 2001

Slowness Anomalies from Two Dense Seismic Arrays at Deception Island Volcano, Antarctica

by G. Saccorotti, J. Almendros, E. Carmona, J. M. Ibáñez, and E. Del Pezzo

Abstract In this article, we analyze the data collected by two short-period seismic arrays deployed at Deception volcano, Southern Shetland Islands, Antarctica. The field survey was conducted during the 1998–1999 austral summer and was aimed at a quantitative assessment of the complex wave fields associated with the magmatic and hydrothermal activity of the volcano. The two arrays had apertures of 320 m and 240 m and were separated by a distance of about 3 km. During the experiment, the arrays recorded several regional earthquakes related to the dynamics of the Bransfield Strait and adjoining areas and local volcano–tectonic earthquakes. Seismograms of earthquakes recorded at regional distances reveal a marked difference in the apparent velocities measured at the two array sites. We investigate the causes and implications of these anomalies by first comparing the effectiveness of estimating the horizontal slowness vector using three different techniques: the multiple signal classification (MUSIC) approach, the zero-lag cross correlation (ZLC) method, and plane-wave fitting to *P*-wave arrival times. While each technique provides the same horizontal slowness vector as the most likely estimates, the plane-wave fitting is associated with the most robust definition of measurement uncertainties. We then investigate the dispersive properties of Rayleigh waves in the 1–8 Hz frequency band at both arrays and invert the two dispersion curves for a shallow velocity structure. The results indicate a marked difference in the seismic velocities for the shallower 200 m beneath the two sites. This may be reconciled with the observed wave vector anomalies by assuming the existence of a sharp lateral velocity heterogeneity, the effect of which would be to bend downward rays impinging at the northernmost array. The reliability of this hypothesis is verified by computing finite-difference wave fronts in a 2D heterogeneous medium. Based on the morpho-structural characteristics of the volcano, the inferred velocity discontinuity maybe associated with the ring-fracture system bordering the collapsed caldera structure that extends over the inner part of the island.

Introduction

Deception Island (62°59′ S, 60°41′ W), located northwest of the Antarctic Peninsula, is the main active volcano of the marginal trench of the Bransfield strait (Fig. 1a). Its main volcano–tectonic feature is the large (8 × 12 km), ellipsoid-like depression flooded by the sea (Fig. 1b), which has been interpreted as a caldera (Baker *et al.,* 1975). Most of the recent volcanic activity has occurred in the close neighborhood of the rims of this depression.

The first digital seismic observations at Deception Island date back to 1986, and through 1993 the measurements have been limited to sparse networks of a few stations. These earlier experiments allowed for seismic-based monitoring of volcanic activity (Ortiz *et al.,* 1997) and for investigations about the location and temporal recurrence of local earthquakes (Correig *et al.,* 1997). Since 1994 the island has been monitored during the austral summers using a dense, small-aperture array located in the close neighborhood of the Spanish Antarctic Base Gabriel De Castilla (see Fig. 1b). These observations allowed for detailed investigations about the spatial distribution of regional earthquakes (Ibañez *et al.,* 1997) and offered new glimpses for interpreting the source processes of the local seismicity related to magmatic and hydrothermal activity (Alguacil *et al.,* 1999; Almendros *et al.,* 1997, 1999; Ibañez *et al.,* 2000). The intriguing results obtained from these latter studies also suggested the need for extending dense-array observations to other sectors of the island, with special reference to the northern inner shore of the caldera, where the most recent eruptive activity oc-

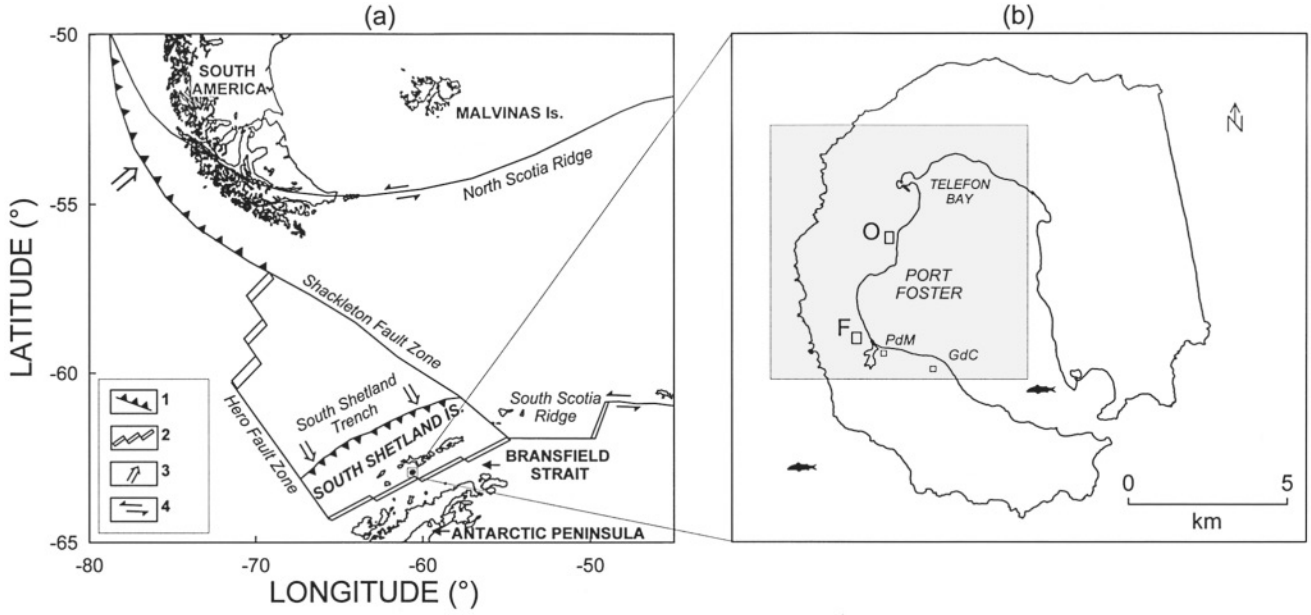

Figure 1. (a) Schematic tectonic map of the South Shetland Islands and Bransfield Strait between South America and the Antarctic Peninsula (modified from Grad *et al.,* 1997). (1) Subduction trench; (2) divergent plate boundary, ridge and transform faults; (3) direction of subduction; (4) relative motion at the plate boundary. (b) Sketch map of Deception Island with location of Spanish Base Gabriel de Castilla (GdC) and the Argentinian Base Primero de Mayo (PdM). Gray boxes mark the location of the arrays deployed during the austral summer 1998–1999; the two labels O and F indicate the Obsidiana and Fumarola sites, respectively. Telefon Bay is the site where the most recent (1967–1970) eruption activity occurred. The shaded rectangle marks the area depicted in Figure 7.

curred. This goal was attained with the 1998–99 survey, during which two seismic arrays were deployed at distances of about 2 and 5 km from the western edge of the eruptive fissure where the 1967–1970 eruptions originated (Fig. 1b).

The main advantage offered by seismic arrays over the classical distributed networks is that the joint estimate of slowness vector at the two arrays allows for source location, even for signals (such as volcanic tremor and long-period events) for which the identification of the arrival times of distinct body wave phases is generally impossible. These location procedures are based on the premise that arrays can accurately determine the direction and incidence of incoming seismic energy; the source of seismic waves is then determined by projecting back along this direction. The accuracy of any such location, therefore, will depend upon the nature of local heterogeneity between the source and receiver, inasmuch as such heterogeneity will cause seismic rays to deviate from their predicted paths. Hence, the usefulness of an array in this type of application will depend upon an ability to characterize and correct for these effects.

In this article, we present evidence for a marked slowness anomaly observed by the 1998–1999 array deployments. Although we hypothesize this anomaly to be related to the Deception caldera collapse, thorough modeling of the complete data sets of slowness and azimuth information from local seismicity is reserved for a subsequent article.

This work is structured into five sections: (1) description of the array deployments and the collected data set; (2) comparison and discussion of three different approaches for estimating the horizontal slowness vector from array data; (3) observations of significant *P*-wave slowness (~0.3 sec/km) and azimuth (up to 100°) anomalies from a selection of eight regional earthquakes; (4) investigation of the shallow velocity structure beneath the two arrays using the dispersion properties of Rayleigh waves as inferred from application of Aki's (1957) correlation method; and (5) discussion of the two velocity models and slowness anomalies in the framework of the volcano–tectonic feature of the island.

Array Setup and Instrumentation

The selection of the sites for the installation of the two arrays was mostly constrained by the rough topography and the accessibility for array maintenance and data retrieval. The first array was installed at the Obsidianas beach, about 2 km SSE of the craters formed during the 1967–1970 activity (see Fig. 1b). This array consisted of 14 stations deployed along two concentric semicircles with radii of 160 and 80 m, respectively (Fig. 2a). Stations at the external and internal semicircle were spaced by angular intervals of about 26° and 45°, respectively, with respect to the hub of the array. The station at the hub of the array was equipped with

a three-component, L-15 Mark Products sensor. All other stations were equipped with vertical-component, L-15 Mark Products sensors, with a natural frequency of 4.5 Hz. Electronic extensions allowed all the sensors to achieve a flat response curve in the 1–50 Hz frequency interval (Del Pezzo *et al.,* 1997).

The second array was deployed atop an alluvial fan in close proximity to the Fumarolas Bay fumarole system, approximately 500 m NW of the Argentinian base Primero de Mayo (Fig. 1b). This array had an aperture of 240 m with stations located along two semicircles, one of radius 120 m and the other of radius 60 m (Fig. 2b). The angular spacing between stations of the outer semicircle was 45° and was 60° for the inner semicircle. This array was equipped with three Mark Products L-4 three-component sensors having a natural frequency of 1 Hz, and with seven Mark Products L-15 vertical sensors having the same characteristics of those previously described for the Obsidianas array. Sensor positioning at both arrays was determined using the Global Positioning System (GPS), which allowed for a precision in the measurement of relative sensor position of about 1 cm. Recording at each array was performed via two eight-channel, PC-based digital recorders with a dynamic range of 16 bits, recording data at 200 samples/sec/channel. Absolute timing at each recorder was achieved via synchronization with the GPS time code. The instruments recorded in trigger mode from 9 December 1998, through 25 February 1999. In addition, 150-sec-long sections of background noise were periodically collected at both the arrays. The Fumarolas and Obsidianas arrays are hereinafter referred to as the F and O deployments, respectively.

Data Description and Analysis

The data set recorded by the array deployments includes a variety of seismic signals that were classified according to their shape, magnitude, and frequency content. These include noise samples, icequakes, local and regional earthquakes, tremor, and long-period signals. A review of the recent seismic activity at Deception volcano may be found in Ibañez *et al.* (2000).

During the field experiment, we routinely analyzed the array data using the zero-lag cross correlation (ZLC) technique (Frankel *et al.,* 1991; Del Pezzo *et al.,* 1997) in order to quickly retrieve qualitative information about the source backazimuth and depth. Comparison of the results obtained at the two arrays showed that, for a given phase of the same event, the ray parameters estimated at the O array were systematically higher than those observed at the F site. This observation could be explained in terms of different epicentral distances; however, the same discrepancies were observed also for regional events, for which the distances to the source are much greater than the spacing between the two arrays. This implies that no significant difference in the horizontal slowness should be observed at the two sites, if a laterally homogeneous propagation medium is assumed.

In the following, we analyze a set of eight regional ($t_s - t_p > 4$ sec) earthquakes recorded at both the arrays (see Table 1) and discuss the resolution and uncertainties of three different approaches for estimating the direction and apparent velocity with which seismic waves propagate across the antennas. We then use the results of the array analyses to quantify the slowness anomalies.

The earthquakes we consider were recorded by both the arrays between 16 December 1998 and 6 February 1999 (Table 1). Considering the range of observed epicentral distances and source backazimuths (see later in this section), the origin of this seismicity is probably related to the slow underthrusting of oceanic crust at the South Shetland Trench (Grad *et al.,* 1997) (see Fig. 1a). All the events are characterized by excellent signal-to-noise ratios, which allow for minimum uncertainty in the picking of both *P* and *S* waves (Fig. 3a).

Three distinct approaches are commonly used to estimate slowness and azimuth from an array of sensors: (1) time- or frequency-domain wave field decomposition techniques; (2) plane-wave fitting to first arrivals, and (3) particle motion analyses. We discarded the latter one for two rea-

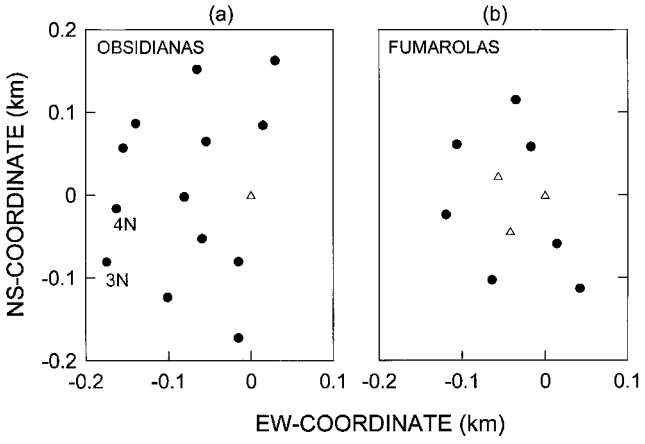

Figure 2. Configuration of the arrays deployed at (a) Obsidianas and (b) Fumarolas sites. Solid dots mark vertical component sensors, triangles indicate three-component stations.

Table 1
Description of the Earthquakes Used in This Study

Event ID	Date (mm-dd-yyyy)	Time at Start of Record (F-array, GMT)	T_s–T_p: O array (sec)	T_s–T_p: F array (sec)
3500250	12-16-1998	02:50:46	7.3	6.5
3582201	12-24-1998	22:01:58	8.4	7.8
3641216	12-30-1998	12:16:49	6.7	6.7
0031812	01-03-1999	18:12:17	11.5	11.3
0210853	01-21-1999	08:53:52	5.1	4.7
0270655	01-27-1999	06:55:20	11.6	11.6
0331550	02-02-1999	15:50:20	4.3	4.1
0370028	02-06-1999	00:28:46	11.4	11.6

sons. The first is that we observed the *P* waves to impinge at the F array almost vertically, thus making the estimate of the azimuth of the principal axis of the polarization ellipsoid extremely difficult (see Figs. 3c, d). The second is associated with the reduced number of three-component stations, which prevented us from using multiple-station averaging techniques (e.g., Jurkevics, 1988) aimed at smoothing the effects induced on particle motion by local heterogeneities beneath the array.

Among the numerous methods for decomposing the elastic-wave field observed by an array of sensors into a linear combination of plane waves, we select and compare the performance from application of (1) the multiple signal classification (MUSIC) technique (Goldstein and Archuleta, 1987, 1991) and (2) the ZLC technique (Frankel *et al.,* 1991; Del Pezzo *et al.,* 1997). In testing these techniques, we consider the first arrival of the event 3500250 as recorded at the O array. The results from this procedure are displayed in Figure 4, where the slowness spectra obtained from application of these techniques are compared to those derived from the plane-wave fitting to first arrivals, or the beamforming method. The slownesses estimated from application of these three approaches are basically the same and indicate a *P* wave propagating to an azimuth of about N80°W and ray parameter of about 0.5 sec/km. Nevertheless, two reasons make us favor the plane-wave fitting approach. The first is that both the ZLC and MUSIC methods are applied over a window of signal, thus inviting the undesired possibility of extending the analysis over multiple, delayed arrivals following the first *P*-wave pulse. The second is that neither of these techniques provides a quantitative assessment of the errors associated with the estimate of the slowness vector, a topic that becomes crucial once measurements from two distinct arrays are compared.

Conversely, the plane-wave fitting allows for a robust estimate of the uncertainties associated with the inversion procedure: the two components of the *P*-wave slowness vector are in fact expressed through a probability density function $P(\mathbf{S})$, which is obtained from the maximum-likelihood expression (Menke, 1989):

$$P(\mathbf{S}) = K \cdot \exp\left[-0.5 \sum_{i=1}^{N} (t_i - \mathbf{S}\cdot\mathbf{x}_i)^2/(\sigma_M^2 + \sigma_{D_i}^2)\right] \quad (1)$$

where the $\mathbf{x}i$ are the coordinates of the N array stations with respect to a reference sensor, and t_i and $\sigma_{D_i}^2$ are the arrival times and picking errors at the different array elements, respectively. σ_M^2 is the error in the prediction of travel times at the array sensors associated with local velocity heterogeneities beneath the array, and K is a normalization factor.

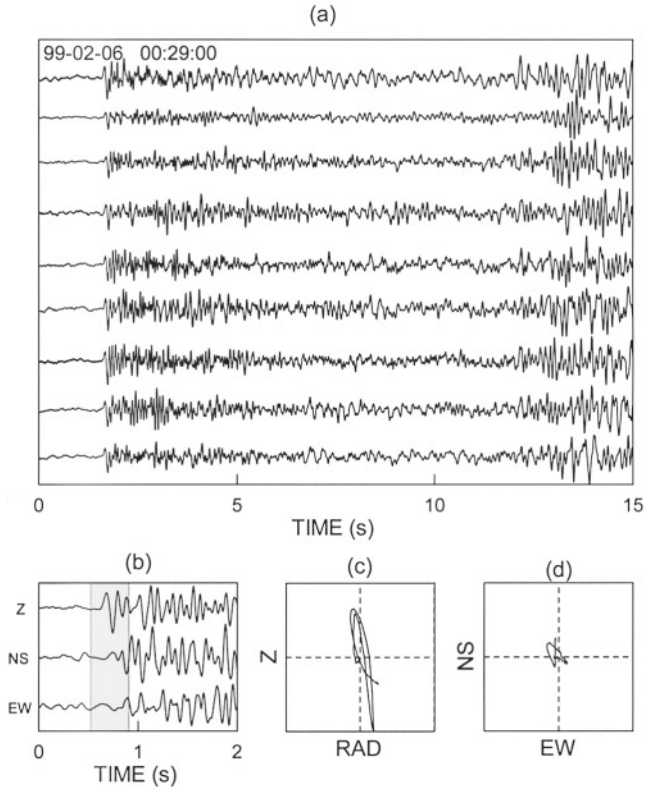

Figure 3. (a) Ground velocity recordings of the event 0370028 (see Table I in text) from the vertical sensors of the F array. Seismograms are arranged in no particular order. Date and time at the start of the recordings are indicated at the upper left. (b) Three-component seismograms from station F1, located at the hub of the F array. Traces have been band-pass filtered in the 1–10 Hz frequency band using a 5-poles, 0-phase-shift Butterworth filter. The shaded area marks the interval selected for the particle motion analyses depicted in (c) and (d). (c),(d): *P*-wave particle motion plots projected on the radial–vertical (c) and horizontal (d) planes, respectively.

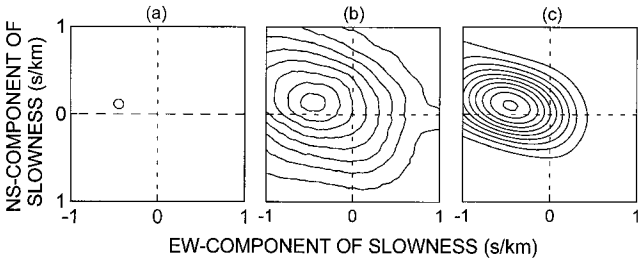

Figure 4. *P*-wave slowness spectra for the event 3582201 as recorded at the O array. The different spectra have been derived from application to the *P*-wave pulse recorded at the array of (a) the plane-wave fitting to *P*-wave arrival times, (b) the ZLC technique, and (c) the MUSIC method. The outer contour line of the spectrum in (a) marks the 90% confidence interval in the estimate of the two components of the slowness vector. The two spectra in (b) and (c) have been calculated over a 1.28-sec-long window encompassing the *P*-wave and in the 1–10 Hz frequency band. In all the three maps, the component of slowness have been reversed in sign, so that the peaks indicate source backazimuth.

The search for the signal slowness is conducted by maximizing equation (1), which is solved numerically by performing a grid search over a range of trial slownesses **S**, for which the predicted travel times at the different sensors are calculated.

Figure 5 shows the results of the plane-wave fitting analysis for the eight earthquakes recorded at the O and F arrays. Given the extreme precision with which it was possible to pick the *P*-wave onset, as well as the reduced aperture of the arrays, the calculation is made by setting the parameters σ_D and σ_M of equation (1) equal to 0.005 sec (1 time sample) and 0.01 sec, respectively. In these maps, the *P*-wave slownesses are represented by the 90% confidence bounds in the estimate of equation (1), and the (x, y) components of vector slowness are taken relative to a Cartesian system oriented E-W–N-S. As in Figure 4, the representation has been made by reversing the sign of the two components of vector slowness so that the peak values of the maps display source backazimuth. For all the cases taken into account, we note a systematic difference among the slownesses observed at the two array sites. Since these differences are significatively greater than the error bounds on the measurement procedures, we conclude that the two arrays measure two different portions of a deformed wave front. This observation is discussed in the last section, with reference to the morpho-structural features of the island.

Shallow Velocity Models

The shallow velocity structures beneath the two antennas are evaluated from the dispersive properties of the surface waves composing the noise wave field. We measure phase velocities of Rayleigh waves using the spatiotemporal correlation technique designed by Aki (1957) for the analysis of stationary stochastic wave fields. Assuming that the noise represents the sum of horizontally propagating waves with the same phase velocity for a given frequency and that the waves propagating in different directions are statistically independent, Aki's method provides a relation between the spectrum of the waves in time and their spectrum in space.

In the following, we first review the spatial correlation representing the vertical component of the two-dimensional wavefield, and follow with the data analyses and interpretation. Finally, a surface velocity structure is derived for beneath the two different arrays.

Aki's correlation method is introduced by first defining a spatial correlation function, $\phi(r, \varphi)$, as

$$\phi(r, \varphi) = \langle u(x, y, t)u(x + r\cos\varphi, y + r\sin\varphi, t)\rangle \quad (2)$$

where $u(x, y, t)$ is the ground velocity observed at point (x, y) and time t; r is the station separation; φ is the station azimuth measured counterclockwise from the x (E–W) axes, and $\langle\ \rangle$ denotes the ensemble (time) average. The azimuthal average of this function is given by

$$\bar{\phi}(r) = \frac{1}{\pi}\int_0^{\pi} \phi(r, \varphi)d\varphi. \quad (3)$$

For the vertical component, the power spectrum, $P(\omega)$, can be related to $\bar{\phi}(r)$ via J_0, the zeroth-order Bessel function:

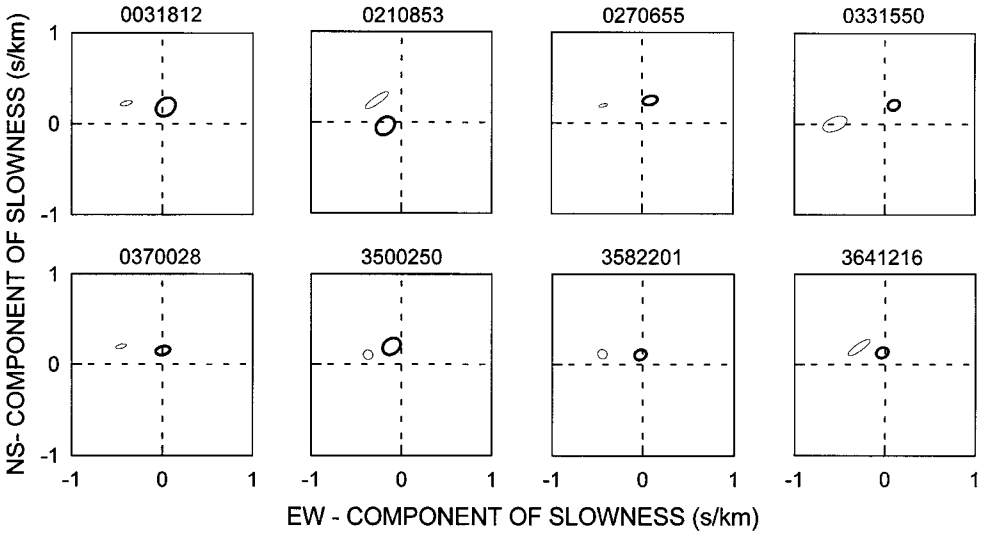

Figure 5. Slowness spectra evaluated at the F (bold lines) and O (thin lines) arrays from plane-wave fitting to *P*-wave arrival times for the eight earthquakes listed in Table I. In all the maps, the contour bounds the 90% confidence interval in the estimate of the slowness vector. The event IDs are reported at the top of each plot. As in Figure 4, the two Cartesian components of vector slowness have been reversed in sign, so that the peaks of the spectra indicate source backazimuth.

$$\bar{\phi}(r) = \frac{1}{\pi} \int_0^\infty P(\omega) J_0 \left(\frac{\omega}{c(\omega)} r \right) d\omega \quad (4)$$

where ω is the angular frequency and $c(\omega)$ is the frequency-dependent phase velocity. Filtering the waves through a narrowband filter centered at frequency ω_0 simplifies equation (4) to

$$\bar{\phi}(r, \omega_0) = P(\omega_0) J_0 \left(\frac{\omega_0}{c(\omega_0)} r \right). \quad (5)$$

Then, introducing a normalized correlation coefficient as

$$\rho(r, \omega_0, \varphi) = \frac{\phi(r, \omega_0, \varphi)}{\phi(0, \omega_0, \varphi)}, \quad (6)$$

we obtain its azimuthal average as

$$\rho(r, \omega_0) = J_0 \left(\frac{\omega_0}{c(\omega_0)} r \right). \quad (7)$$

Thus, phase velocity can be estimated from measurements of correlation functions for vertical motion from a semicircular array. Equation (7) is valid for the vertical component of motion, which consists of *P–SV* motion. Assuming that ambient noise is composed mainly of surface waves, the results from application of these equations can be interpreted as an estimate of Rayleigh wave phase velocities. This technique has been used by Ferrazini *et al.* (1991) to study the characteristics of shallow tremor and gas-piston events at Puu Oo crater, Hawaii; by Métaxian *et al.* (1997) to analyze the wave field properties of permanent tremor at Masaya volcano, Nicaragua, and by Chouet *et al.* (1998) to infer a shallow velocity structure at Stromboli volcano, Italy.

In our analyses, we first select 120-sec-long time series of background noise recorded at all the stations of the arrays. The seismograms from each station of the array are then Fourier transformed, and the complex spectrum is windowed using a 0.5-Hz-width cosine-taper function. We then calculate the inverse Fourier transform and, once back in the time domain, estimate the ZLC coefficient of the signal from the station located at the hub of the array and the stations located at the two semicircles. The frequency-dependent correlation coefficients thus obtained are finally averaged among stations located at the same distance from the hub of the array. This procedure is then repeated by shifting the frequency window with 0.25-Hz steps, in the 0.5–8 Hz interval. To improve the significance of the estimates, we processed six different noise windows, recorded between 10–17 December for the O array and 15–27 December for the F array, and separately averaged the results obtained at the two sites.

The frequency dependence of the azimuthally averaged correlation coefficient for the internal and external semicircles of the O and F arrays, respectively, are shown in Figure 6a. The inferred stationarity of the wave field over the time period spanned by our data windows is verified through the similarity of the correlation functions evaluated for the different intervals. In analyzing data from the external semicircle of the O array ($r = 160$ m), we omitted station 3N (see Fig. 2a), whose distance from the hub of the array was significantly different from the average distances of the other stations.

We then derive the frequencies corresponding to the maxima, minima and zero crossings of the average of the correlation functions shown in Figure 6a. These values are set equal to the corresponding arguments of the zeroth order Bessel function of equation (7), eventually deriving values of the frequency-dependent phase velocity $c(\omega)$. Following the procedures described in Ferrazzini *et al.* (1991) and Chouet *et al.* (1998), we evaluate the errors on such estimates to be about 10%. This procedure gives a more conservative evaluation of the uncertainties as if we had considered the sample standard deviation of the correlation coefficients calculated over the different recordings. The results from this procedure are depicted in Figure 6b, where the dispersion characteristics at the two arrays are shown. These two different data sets are then least-square fitted by a relationship of the form (Chouet *et al.,* 1998):

$$c(f) = A \cdot f^{-a} \cdot e^{bf} \quad (8)$$

where f is the frequency in Hz ($f = \frac{\omega}{2\pi}$) and A, a, and b are constants. For the O site, $A = 0.4$, $a = 0.86$, and $b = 0.13$; for the F site, $A = 2.8$, $a = 2.4$ and $b = 0.35$.

These dispersion functions are then inverted for the corresponding velocity structures under the assumption that those dispersions represent the fundamental modes of Rayleigh waves. Our search for structural models that produce phase velocities compatible with the experimental dispersions is conducted using both a trial-and-error approach and an inversion procedure based on the computer codes developed by Hermann (1987). For each array site, we first considered a simple model consisting of a single layer underlain by a homogeneous half-space. The thicknesses of the surficial layers are selected according to the minimum wavelength of Rayleigh waves observed at each site; the velocities of the top layer and the half-space are adjusted to fit the low- and high-frequency limits in the distribution of experimental data. We then fit the curvature of the dispersion data by gradually increasing the number of layers in the model and proceed changing layer thicknesses and velocities until the fit is considered satisfactory. This structure is then used as a starting model for the inversion procedure, which is iterated until the rms between the observed and predicted dispersion curves is smaller than a given threshold, set equal to 0.05. The velocity models at the two array sites resulting from this procedure are illustrated in Figure 6c, while in Figure 6b the dispersion curves for Rayleigh waves pre-

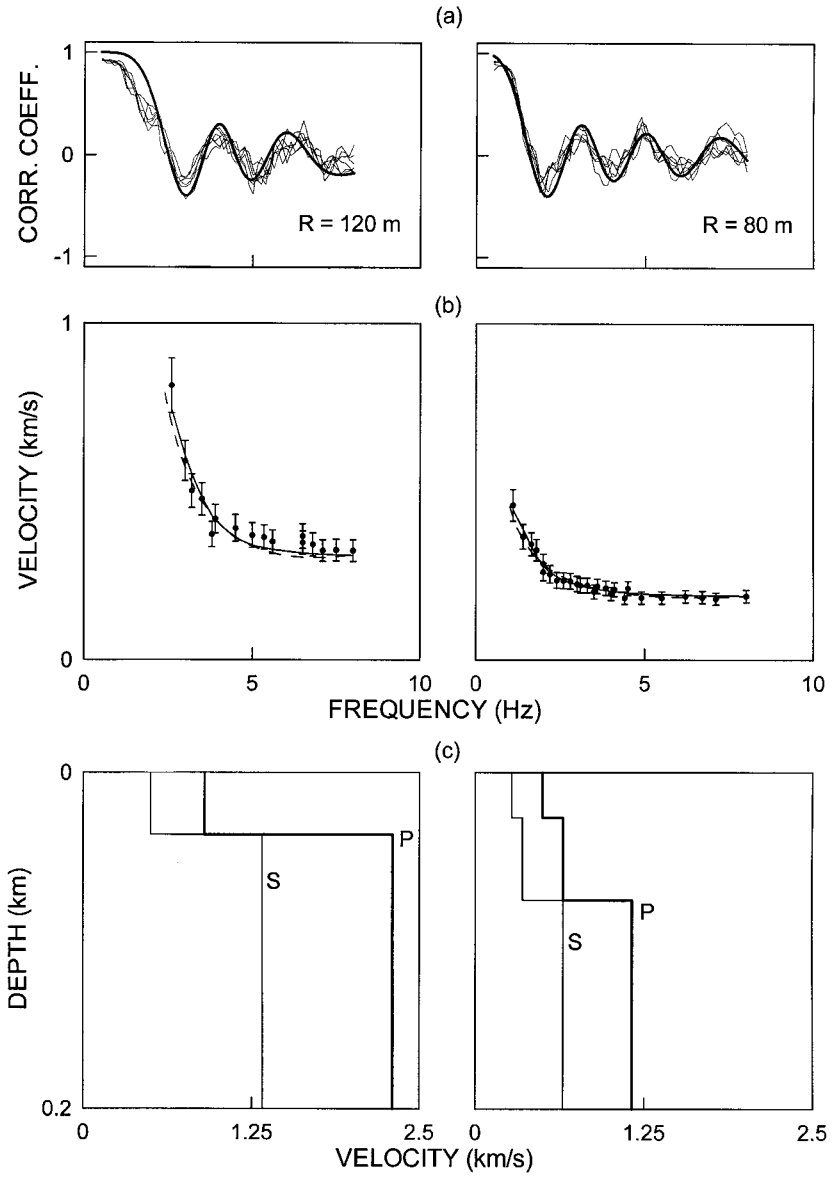

Figure 6. (a) Azimuthally averaged correlation functions for the outer semicircle of the Fumarolas array (left), and the inner semicircle of the Obsidianas array (right). The thick line represents the zeroth-order Bessel function derived from substitution of the dispersion relationship expressed through equation (5) to the phase velocity terms at the right-hand side of equation (4). (b) Phase velocities as a function of frequency for the P–SV component of motion derived at the F (left) and O (right) arrays. Dots represent velocities derived from reading of the zero-crossing, maxima and minima of the average of the correlation functions shown in (a). Dashed lines represent the dispersion functions derived from fitting equation (8) to the velocity data. These functions have been used for deriving the velocity models shown in (c). Dispersion functions predicted from these models are represented by the continuous lines. (c) *P*- (bold lines) and *S*- (thin lines) velocity structures for the F (left) and O (right) sites, derived from inversion of the Rayleigh waves dispersion data depicted in (b).

dicted from these structures are compared to the experimental phase velocities.

The F array is characterized by a ~40-m-thick surficial layer, whose *S*- and *P*-wave velocities are 0.5 and 0.9 km/sec respectively. These values are compatible with the sediments of the talus resulting from erosion of the caldera rim over which that array was deployed. The half-space underneath the shallowest layer is characterized by *S*- and *P*-wave velocities of about 1.3 and 2.3 km/sec respectively, in agreement with the larger scale crustal model derived by Grad *et al.* (1993) from analysis of refraction and wide-angle reflection data.

The two shallower layers at the O site are characterized by *S*- and *P*-wave velocities ranging in the 0.27–0.35 and 0.5–0.65 km/sec intervals, respectively. The half-space at that site depicts *S*- and *P*-wave velocities of 0.65 and 1.2 km/sec, respectively. These velocities are thus roughly half of those derived for the same range of depth at the F site.

The differences among the two sites for the shallower layers can be easily interpreted in light of the surface geology: the O array was in fact deployed onto a sandy epiclastic deposit of marine origin, whose shear modulus is expected to be significatively lower than that of the consolidated sediments beneath the F array.

More difficult is interpreting the differences observed at greater depths. Based on considerations about the penetration depths of the high-frequency surface waves used to derive the models, we estimate the validity of our measurements to extend down to depths of about 150–200 m. This thickness is obviously too great to be attributed solely to the sandy deposits without invoking any kind of structural control on the sedimentary processes. This evidence will serve

us to better interpret the slowness anomaly in the framework of the structural evolution of the volcano.

Discussion and Conclusions

In this article, we analyze ray parameters and backazimuths for a set of eight regional earthquakes recorded by a double-array deployment at Deception Island volcano, Southern Shetland Islands, Antarctica. Results from our measurements indicate that the *P*-wave pulse from the same earthquake is observed at the two sites with a significant difference in the apparent (horizontal) slowness. For most of the cases we analyzed, the source-to-receiver distance is much greater than the separation between the two arrays, thus implying that the slowness discrepancies cannot be attributed to different epicentral distances. We must therefore hypothesize that seismic rays traveling to the two arrays sample portions of the crust characterized by different seismic velocities. Two reasons constrain this lateral velocity discontinuity to be located in close proximity of one of the two arrays. The first is that vector slowness data are most sensitive to velocity structure near the receiver (see Figure 1 by Hu *et al.,* 1994); the second, is that this discontinuity has to be sampled selectively by only one of the two rays: this occurs if the two rays are separated by a sufficient distance, a condition that is achieved only in the terminal part of the ray paths.

A major question remains with regard to the location and extent of such heterogeneity. A difference between the present work and similar studies done in the past (e.g., Steck and Prothero, 1993; Lin and Roecker, 1996) is that for the earthquakes we analyze, no independent locations are available: to our knowledge, the eight events we considered were not recorded by any other seismic network. This means that the slowness data at our arrays cannot be compared to any prediction derived from an independent knowledge of the source location. Thus, the slowness anomalies we refer to must be analyzed as relative anomalies between a pair of observations, rather than discrepancies with respect to values predicted for a given hypocenter and velocity structure. In the previous analysis, we implicitly assumed the F array to be unaffected by slowness anomaly. This choice was motivated by the fact that the ray parameters we observed at that particular site were compatible with *P*-wave propagation from distant sources. In fact, the ray parameter observed by an array is constant throughout the ray path and corresponds to the inverse of the seismic velocity at the turning point of the ray. In the case of the O array, this would imply that P waves propagating from sources as far as 80–100 km would sample layers with velocities not exceeding 2 km/sec, which is obviously unrealistic. Taken together, these considerations seem to indicate that the velocity heterogeneity is located in close proximity to the O array and that its geometry and extent must be able to cause a downward bending of seismic rays impinging at that particular site from a range of backazimuths spanning the NW quadrant (see Fig. 5). To that purpose, a vertical or quasi-vertical impedance contrast could represent a reasonable interpretation: rays traveling through the higher-velocity region would be severely bent downward as they transmit across the interface to the low-velocity region.

From correlation analysis of selected records of seismic noise, we calculated the dispersive properties of Rayleigh waves, from which a shallow velocity model at the two array sites was obtained. The shallow velocity model derived for the F site is compatible with the regional crustal structure, except for the shallowest, 40-m-thick low-velocity layer. The concordance between the shallow velocity structure at the F site and the larger scale, regional model lends additional support to the idea that the anomalous ray propagation only affects the O array. Conversely, this latter site is characterized by a shallow velocity structure whose *P*-wave velocity is about one-half of that inferred for the F site. As indicated by the right bottom panel of Figure 6, the low-velocity zone beneath the O array appears to extend to a depth of at least 150 m. It is quite unlikely that the lens of loose epiclastic deposits, where that array was deployed, reaches such a thickness. Therefore, the low-velocity zone evidenced by our measurements has to be related to some structural depression successively filled by volcanoclastic and/or sedimentary deposits.

These observations and this hypothesis may be collected into a coherent picture, once one considers the structural and volcanological features of the island. Figure 7a reports a shaded relief map of the N–NW sector of the volcano encompassing the F and O sites. The principal morpho-structural characteristic is represented by the large ellipsoid-like depression (caldera), whose rims are crossed by faults dislocating the entire structure in discontinuous blocks (De Rosa *et al.,* 1995). However, geomorphological considerations (G. Ventura, personal comm., 1999) suggest that the caldera walls suffered major erosion, thus implying that the present-day caldera rims are displaced outward with respect to the fracture systems along which the collapse occurred.

The inner (submerged) part of the caldera is filled by loose sedimentary and volcanoclastic deposits, whose *P*-wave velocities range between 0.5 km/sec for the shallowest 20 m, to 1.4 km/sec for an underlaying layer that extends down to a depth of about 500–600 m, as indicated by a refraction survey conducted by Ortiz *et al.* (1989). These velocities are thus compatible with those obtained in the present study from Rayleigh wave dispersion data at the O site. The most recent eruptive activity (e.g., 1967 and 1970 eruptions) is located on a system of discontinuities trending NE–SW, which are very probably associated with the structures along which the inner part of the volcano collapsed. Moreover, data from a recent bathymetric survey (DECVOL Team, personal comm., 2000) indicate that a 200-m-high, NNW–SSE-oriented fault scarp is located a few hundreds of meter offshore the F site.

Taken together, these considerations allow us to estimate an approximate distance of about 1 km between the

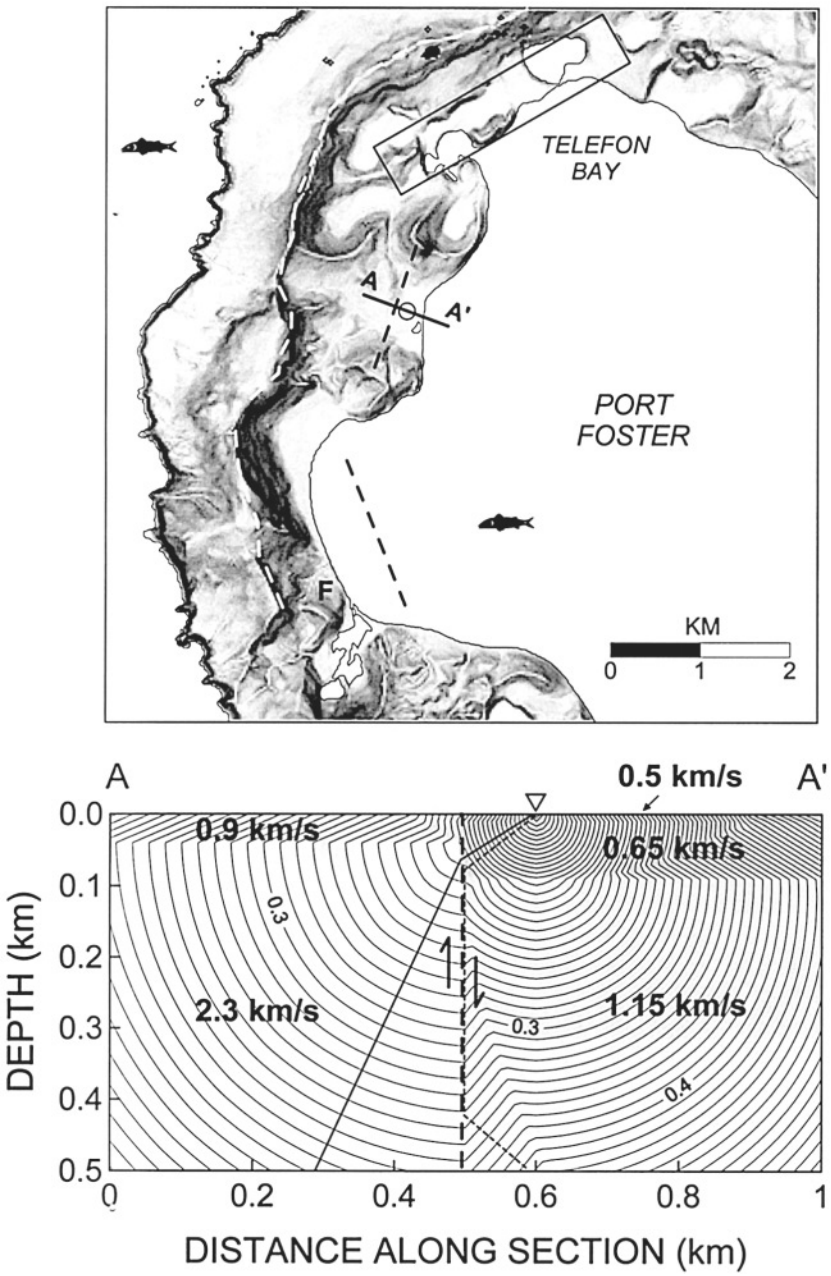

Figure 7. (a) Shaded relief map of the area encompassing the O and F arrays. This area corresponds to the rectangle in Figure 1a. The white dashed line onshore corresponds to the rim of the caldera. The rectangle at Telefon Bay bounds the region where the 1967–1970 phreato-magmatic and strombolian eruptions occurred. The dashed line offshore the F site marks the approximate position of a fault scarp imaged by a recent bathymetric survey. The A–A′ line marks the profile through which passes the cross-section depicted in (b). This line bisects the inferred fault associated to the caldera collapse (dashed line). The location of the hub of the array is marked by a circle. (b) Schematic model of the cross-section along profile A–A′ shown in (a). The triangle at the top of the map indicates the location of the array. *P*-wave velocities are indicated by different shading and bold numbers. Contour lines corresponds to the isochrones (wave fronts) for a source located at the hub of the array. Contour interval is 0.01 sec. The bold black line indicate a seismic ray impinging at the discontinuity with an incidence angle of about 30°. Note the deflection of the ray after having passed through the velocity interface. The dotted line indicates a ray coming from SE and refracted at the discontinuity. In that case, the backazimuth observed at the array points to a direction which is opposite to that of the source.

present-day caldera rims and the main fracture system along which the collapse occurred. According to this picture, and remembering the concordance of the velocity models at the F and O sites with the regional and inner caldera structures, respectively, we may conclude that the F array was deployed over the body of the old volcano edifice, while the O array was deployed over the collapsed part of the caldera successively filled by volcanoclastic and marine deposits. The F and O arrays would thus be located west and east, respectively, of the fracture system associated with the caldera formation.

To verify whether this hypothesis is compatible with the observed slowness anomalies, we examine the geometry of seismic rays propagating in a 2D, heterogeneous medium. Using the finite-difference approach of Podvin and Lecomte (1991), we use travel-time reciprocity and calculate the wave fronts of seismic waves that emanate from a source located at the O array and propagate through a laterally heterogeneous structure. The results from this simulation are illustrated in Figure 7b, where a vertical section orthogonal to the inferred fault trace is displayed. The trace of the fault is taken to be at a distance of about 1 km from the caldera rim and parallel to it. The velocity structures west and east of the fault are assumed to be those previously inferred for the F and O site, respectively. The figure clearly shows that, for a wide range of incidence angles (say, from 90° to 45°), wave

fronts impinging at the O array are severely bent downward by the subvertical interface, with a net decrease of the apparent velocity as the waves impinge at the surface. It must be stressed that the observations discussed thus far are not sufficient to definitively validate the proposed model. The lack of additional recordings of regional earthquakes spanning a wider range of backazimuths hinders the possibility of ruling out other effects, as for instance a strong diffraction west of the O array. However, three considerations lend support to our model. The first is the dependence of the observed slowness anomalies on the inferred source backazimuth. If the anomalies were due to the radiation from a strong, near-receiver diffractor, then the O array should always measure the backazimuth to this latter one, independently of the backazimuth to the primary source. Conversely, as displayed in Figure 5, the magnitude of the anomaly appears to be strongly dependent on the inferred source backazimuth. The second is the ability of the model to reconcile the observations with the surface geological features and seismic velocity distributions. The third, is related to the data of local earthquakes that occurred from late December 1998 through February 1999 below Port Foster (see Fig. 7a), 1–4 km NE of the F array. For these events, we observed the same backazimuth discrepancies among the two arrays as those previously observed for regional sources (Fig. 8). If the anomalous slowness of first arrivals observed at the O array for regional sources located north-northwest of the island were due to a diffractor, than that anomaly shouldn't be observed in the case of local earthquakes originating SSE of the same array. In light of the model proposed in Figure 7b, the persistency of the anomaly for these latter sources could be representative of head waves that travel along the vertical discontinuity and then turn back toward the array as they impinge at the free surface (dotted line in Fig. 7b). More quantitative constraints about the nature of the inferred velocity discontinuity and its spatial setting imply the need for a detailed analysis of the data set from local seismicity, which in turn requires the joint inversion of slowness measurements for both source location and 3D velocity structure. Such a complex process (called *polarization tomography* after Hu *et al.,* 1994) is an effort that goes beyond the purpose of the present article and is reserved for a subsequent study.

A major lesson is taken from the present work. Over the past 15 years, array techniques have progressively become more popular among seismologists faced with the analysis and interpretation of signals associated with volcanic activity (e.g., Goldstein and Chouet, 1994; Chouet *et al.,* 1997; Del Pezzo *et al.,* 1997, and references therein). Multichannel methods have been demonstrated to be a powerful tool for quantifying the kinematic properties of the complex wave fields observed in active volcanic environments, such as volcanic tremor, long-period events, and signals associated with mechanism of degassing in open vents. However, volcanic edifices are characterized by extremely complex tectonic features, resulting from the superposition of regional stresses and local, heterogeneous stress fields. The distribution of seismic velocities reflects these complexities, and variations of several tenths of a percent in both compressional and shear velocities are common over distance scales on the order of a few hundred meters. Any source localization procedure, based on the back propagation of seismic rays through a more or less defined velocity structure, should therefore account for these heterogeneities and their spatial distribution.

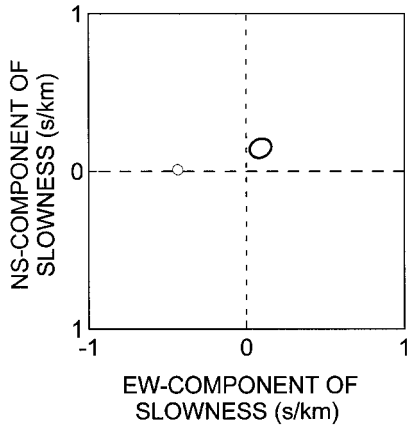

Figure 8. Slowness spectra evaluated at the F (bold line) and O (thin line) arrays for a local earthquake that occurred on 30 December 1998, at 14:54 UTC. The estimated S–P times are about 0.7 sec and 1.1 sec at the F and O array, respectively. As in Figures 4 and 5, contouring bounds the 90% confidence level in the estimate of slowness vector, whose Cartesian components have been reversed in sign so that the spectra indicate source backazimuth.

Acknowledgments

Thoughtful comments from Rick Aster, Mike Hagerty, and an anonymous reviewer greatly helped in improving the quality of the manuscript. The scientific expedition at Deception Island was supported through the project CICYT-ANT98-111 under the Spanish Antarctic Research Program. This work could not have been possible without the logistic and technical assistance of the military staff of the Gabriel de Castilla base. Jaime Potti, Ana de Leon, Juanto Fargallo, Mariano Rodriguez-Arias, and Fernando Calexico are gratefully acknowledged for their friendship and moral support. Tony Lomax made available, through the Internet, Podvin and Lecomte's finite-difference code for calculation of travel times. Guido Ventura provided precious suggestions while attempting to interpret the morpho-structural characteristic of Deception Volcano.

References

Alguacil, G., J. Almendros, E. Del Pezzo, A. Garcia, J. M. Ibáñez, M. La Rocca, J. Morales, and R. Ortiz (1999). Observations of volcanic earthquake and tremor at Deception Island, Antarctica, *Ann. Geofis.* **42,** 417–436.

Almendros, J., J. M. Ibáñez, G. Alguacil, E. Del Pezzo, and R. Ortiz (1997). Array tracking of the volcanic tremor source at Deception Island, Antarctica, *Geophys. Res. Lett.* **24,** 3069–3072.

Almendros, J., J. M. Ibáñez, G. Alguacil, and E. Del Pezzo (1999). Array analysis using circular wave-front geometry: an application to locate the nearby seismovolcanic source, *Geophys. J.* **136,** 159–170.

Aki, K. (1957). Space and time spectra of stationary stochastic waves with special reference to microtremors, *Bull. Earthquake Res. Inst. Tokyo Univ.* **25,** 415–457.

Baker, P., M. Phil, M. Mc Reath, M. Henry, M. Roobal, and T. Davies (1975). The geology of the South Shetland Islands, V: Volcanic evolution of Deception Island, *Brit. Ant. Survey. Scient. Rep.* No. 78, 81 pp.

Chouet, B. A., G. Saccorotti, M. Martini, P. B. Dawson, G. Milana, G. De Luca, and R. Scarpa, (1997). Source and path effects in the wavefields of tremor and explosions at Stromboli volcano, Italy, *J. Geophys. Res.* **102,** 15129–15150.

Chouet, B., G. De Luca, G. Milana, P. B. Dawson, M. Martini, and R. Scarpa (1998). Shallow velocity structure of Stromboli volcano, Italy, derived from small-aperture array measurements of strombolian tremor, *Bull. Seism. Soc. Am.* **88,** 653–666.

Correig, A. M., M. Urquizu, J. Vila, and J. Marti, (1997). Analysis of the temporal occurrence of seismicity at Deception Island (Antarctica): A nonlinear approach, *PAGEOPH* **149,** 553–574.

De Rosa, R., R. Mazzuoli, R. H. Omarini, G. Ventura, and J. G. Viramonte (1995). A volcanological model for the Historical Eruptions at Deception Island (Bransfield Strait, Antarctica), *Terra Antarctica* **2,** 131–165.

Del Pezzo, E., M. La Rocca, and J. M. Ibáñez (1997). Observations of high-frequency scattered waves using dense arrays at Teide volcano, *Bull. Seism. Soc. Am.* **87,** 1637–1647.

Ferrazzini, V., K. Aki, and B. A. Chouet (1991). Characteristics of seismic waves composing hawaiian volcanic tremor and gas-piston events observed by a near-source array, *J. Geophys. Res.* **96,** 6199–6209.

Frankel, A., S. Hough, P. Friberg, and R. Busby (1991). Observations of Loma Prieta aftershocks from a dense array in Sunnyvale, California, *Bull. Seism. Soc. Am.* **81,** 1900–1922.

Goldstein, P., and R. J. Archuleta (1987). Array analysis of seismic signals, *Geophys. Res. Lett.* **14,** 13–16.

Goldstein, P., and R. J. Archuleta (1991). Deterministic frequency–wavenumber techniques and direct measurements of rupture propagation during earthquakes using a dense array—theory and methods. *J. Geophys. Res.* **97,** 6173–6185.

Goldstein, P., and B. A. Chouet (1994). Array measurements and modeling of a source of shallow volcanic tremor at Kilauea Volcano, Hawaii, *J. Geophys. Res.* **99,** 2637–2652.

Grad, M., Gutерch A., and T. Janik (1993). Seismic structure of the litosphere across the zone of subducted Drake plate under the Antarctic plate, West Antarctica, *Geophys. J.* **115,** 586–600.

Grad, M., Shiobara H., Janik T., Guterch A., and H. Shimamura (1997). Crustal model of the Bransfield Rift, West Antarctica, from detailed OBS refraction experiments, *Geophys. J.* **130,** 506–518.

Herrmann, R. B. (1987). *Computer Programs in Earthquake Seismology, Volume 2: Surface Waves Programs,* User's Guide, Department of Earth and Atmospheric Science, St. Louis University, St. Louis, Missouri.

Hu, G., W. Menke, and C. Powell (1994). Polarization tomography for P-wave velocity structure in southern California, *J. Geophys. Res.* **99,** 15245–15256.

Ibáñez, J. M., J. Morales, G. Alguacil, J. Almendros, R. Ortiz, and E. Del Pezzo (1997). Intermediate-focus earthquakes under South Shetland Islands (Antarctica), *Geophys. Res. Lett.* **24,** 531–534.

Ibáñez, J. M., E. Del Pezzo, J. Almendros, M. La Rocca, G. Alguacil, R. Ortiz, and A. Garcia (2000). Seismovolcanic signals at Deception Island volcano, Antarctica: wavefield analysis and source modeling, *J. Geophys. Res.* **105,** 13,905–13,931.

Jurkevics, A. (1988). Polarization analysis of three-component array data, *Bull. Seism. Soc. Am.* **78,** 1725–1743.

Lin, C. H., and S. W. Roecker (1996). *P*-wave backazimuth anomalies observed by a small-aperture seismic array at Pinyon Flat, Southern California: implications for structure and source location, *Bull. Seism. Soc. Am.* **86,** 470–476.

Menke, W. (1989). Geophysical Data Analysis: Discrete Inverse Theory, Academic Press, Inc., New York, 262 pp.

Métaxian, J. P., P. Lesage, and J. Dorel (1997). Permanent tremor of Masaya volcano, Nicaragua: wave field analysis and source location, *J. Geophys. Res.* **102,** 22529–22545.

Ortiz, R., R. Baloix, and E. Carreno (1989). Interpretation preliminar de un ensayo de perfil sismico de refraccion en Port Foster (Isla Decepcion), Presented at the 3rd Spanish Symposium of Antarctic Studies, Madrid, 3–9 September, 1989.

Ortiz, R., A. García, A. Aparicio, I. Blanco, A. Felpeto, R. del Rey, M. Villegas, J. M. Ibáñez, J. Morales, E. Del Pezzo, J. C. Olmedillas, M. Astiz, J. Vila, M. Ramos, J. G. Viramonte, C. Risso, and A. Caselli (1997). Monitoring of the volcanic activity of Deception Island, South Shetland Islands, Antarctica (1986–1995), in *The Antarctic Region: Geological Evolution and Processes,* C. A. Ricci (Editor), Terra Antarctica Publishers, Siena, Italy, 1071–1076.

Podvin, P., and I. Lecomte (1991). Finite difference computation of traveltimes in very contrasted velocity models: a massively parallel approach and its associated tools, *Geophys. J.* **105,** 271–284.

Steck, L. K., and W. A. Prothero Jr. (1993). Observations of direct *P*-wave slowness and azimuth anomalies for teleseisms recorded in Long Valley caldera, California, *Bull. Seism. Soc. Am.* **5,** 1391–1419.

Osservatorio Vesuviano
Via Diocleziano 328, 80124 Napoli, Italy
gilberto@ov.ingv.it
(G.S., E.D.P.)

Instituto Andaluz de Geofisica
Universidad de Granada
Campus Universitario de Cartuja
18071 Granada, Spain
ibanez@iag.ugr.es; ecarmona@iag.ugr.es.
(J.A., E.C., J.M.I.)

Manuscript received 31 May 2000.